

Effect of P addition on nanocrystallization and high temperature magnetic properties of low B and Nb containing FeCo nanocomposites

Rajat K. Roy^{1,2,a)} S. Shen,² S. J. Kernion,² and M. E. McHenry^{2,a)}

¹NDE and Magnetic Materials Group, CSIR-National Metallurgical Laboratory, Jamshedpur 831007, India

²Department of Materials Science and Engineering, Carnegie Mellon University, Pittsburgh, Pennsylvania 15213, USA

(Presented 3 November 2011; received 10 September 2011; accepted 4 October 2011; published online 6 February 2012)

The P content dependencies of the nanocrystallization behaviors and high temperature magnetic properties of the $\text{Fe}_{54.6}\text{Co}_{29.4}\text{Si}_{2.8}(\text{B}_{0.8-\text{Y}}\text{P}_{\text{Y}})_{14}\text{Nb}_1\text{Cu}_1$ ($\text{Y}=0, 0.2, \text{ and } 0.3$) alloys have been investigated. Alloys were prepared by melt spinning and subsequently annealed in an argon atmosphere to induce nanocrystallization. P addition increases primary crystallization temperature (T_{x_1}), thermal stability (ΔT_{x}), and activation energy (Q_{JMA}) for secondary crystallization in as-cast alloys. The saturation induction (B_{s}) of 1.68 T for as-cast P free alloy decreases continuously with the addition of P. However, the soft magnetic properties are enhanced for P added alloys. The XRD pattern reveals that grain refinement increases with increasing P contents. Alloys annealed at 430 °C confirm primary nanocrystallization of α -FeCo in the amorphous matrix, while annealing at 550 °C causes secondary crystallization of other non-magnetic phases as well. The magnetic moment of as-cast and annealed alloys, measured by vibrating sample magnetometry (VSM), has minimum values at two temperatures, labeled T_{c_1} , T_{c_2} , prior to secondary crystallization, corresponding to the ferromagnetic transitions of as-quenched amorphous and residual amorphous phase, respectively. The stabilization of amorphous phase delays primary crystallization, resulting in increase of T_{c_1} for P-rich as-cast alloys. © 2012 American Institute of Physics.

[doi:10.1063/1.3670056]

I. INTRODUCTION

Recently, the development of soft magnetic materials with high induction has been of great scientific and technological interest. Miniaturization of power electronic components demands highly efficient magnetic materials that can be used in power transformers and converters.¹ These materials must have thermal stability and good high temperature magnetic properties to facilitate good performance in severe environments. Several newly developed Fe based soft magnetic nanocomposites exhibit low thermal stability.²⁻⁴ Moreover, the saturation induction of these alloys is within the ranges of 1.24 – 1.58 T, which is less than that of silicon steel.⁵ The desire to increase saturation induction motivated to develop Nb-substituted FeCo based (Fe,Co)-M-B-Cu ($\text{M} = \text{Nb}, \text{Hf}, \text{ or } \text{Zr}$) nanocrystalline alloys, called HITPERM alloys⁶ with high induction and improved soft magnetic properties.⁷ The Nb addition causes the grain refinement in the nanocomposites, resulting in good soft magnetic properties and low power losses. However, Nb is a costly element and reduction in Nb content is more effective in increasing the saturation induction than B-content reductions.⁸ Therefore, it is desirable to design the new alloys with low Nb content and consider substitution of other glass formers. In this research, we investigate the effect of P on the nanocrystallization behavior and high temperature magnetic properties in

some low Nb containing FeCo based alloys. It is observed that the substitution of P for B in Fe based alloys enhances glass forming ability.³ Additionally, the combined effect of P and Cu results in additional grain size refinement providing increased nucleation sites prior to primary crystallization.⁹

II. EXPERIMENTAL DETAILS

Ribbons (#NP0, #NP2, and #NP3) of nominal composition $\text{Fe}_{54.6}\text{Co}_{29.4}\text{Si}_{2.8}(\text{B}_{0.8-\text{Y}}\text{P}_{\text{Y}})_{14}\text{Nb}_1\text{Cu}_1$ with the replacement of B by P ($\text{Y}=0, 0.2, \text{ and } 0.3$) were prepared by a single roller melt spinning. The Fe: Co ratio was kept at 65:35 to optimize saturation induction. Thermal properties were studied using differential scanning calorimetry (DSC) by a Perkin Elmer DSC7. The structure of as-quenched and annealed samples was studied by X-ray diffraction (XRD). The crystalline phase volume fraction (X_{C}) of annealed ribbons was determined by separating the intensity of diffraction patterns into contributions corresponding to the amorphous and crystalline phases, $X_{\text{C}} = I_{\text{C}}/(I_{\text{A}} + I_{\text{C}})$, where I_{C} and I_{A} were the integral intensities for the crystalline and amorphous phases, respectively. The saturation induction (B_{s}) under a maximum applied field of 800 kA/m and the variation of magnetic moments (M) with temperature and time were measured by a Lakeshore vibrating sample magnetometer (VSM). The activation energy (Q_{JMA}) was evaluated from the maximum inflection point (t_{inf}) of dM/dt versus time (t) plot using the Johnson-Mehl-Avrami equation; this method is described elsewhere.¹⁰ The coercivity

^{a)}Authors to whom correspondence should be addressed. Electronic addresses: rajat@nmlindia.org and mm7g@andrew.cmu.edu.

and permeability of annealed ribbons were determined from B-H curves measured with a B-H loop tracer.

III. RESULTS AND DISCUSSION

Figure 1 shows P content dependencies of primary crystallization temperature (T_{x1}), temperature difference between primary and secondary crystallization (ΔT_x), mean grain size (D) of FeCo nanocrystallites, and saturation induction (B_s) for as-cast melt spun and coercivity and permeability for annealed melt spun $\text{Fe}_{54.6}\text{Co}_{29.4}\text{Si}_{2.8}(\text{B}_{0.8-Y}\text{P}_Y)_{14}\text{Nb}_1\text{Cu}_1$ ($Y=0, 0.2,$ and 0.3) alloys. As-cast alloy ribbons are heteromorphous with the distribution of FeCo nanocrystallites in the amorphous matrix. The nanocrystallite size of alloy #NP2 (2.8 at % P) is comparable to that of alloy #NP0 (0 at % P), however, the crystallites become finer with the addition of 4.2 at % P. The primary crystallization temperature (T_{x1}) and thermal stability (ΔT_x) are also enhanced in the alloys of higher P. The saturation induction (B_s) of 1.68 T for as-cast P free alloy decreases continuously with the addition of P. However, the P content dependence of coercivity (H_c) and permeability (μ) is markedly enhanced in the annealed (430 °C/1 h) alloys. The coercivity rapidly decreases from 250 A/m for alloy #NP0 to 70 A/m for #NP3 alloy. Simultaneously, the permeability of #NP3 becomes twice that of #NP0. The improvement of soft magnetic properties is due to the refinement of grain structure with P addition.

Figure 2 shows the x-ray diffraction patterns of alloys annealed at 430 and 550 °C. After annealing at 430 °C for primary crystallization, the alloys show characteristic α -FeCo peaks along with a broad amorphous halo, consistent with a distribution of α -FeCo nanocrystallites in the residual amorphous matrix. On further annealing, the redistribution of atoms causes the decrease in residual amorphous matrix and the secondary crystallization of other non-magnetic phases along with the α -FeCo phase. Secondary crystallization products include $(\text{FeCo})_{23}\text{B}_6$, $(\text{FeCo})_2\text{B}$ in all three alloys, and a $(\text{FeCo})_2\text{P}$ phase in alloys #NP2 and #NP3. P addition also affects volume fraction and size of the nanocrystallites during

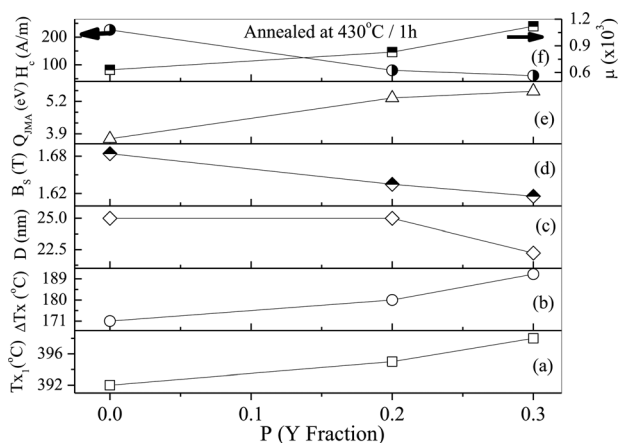


FIG. 1. Compositional dependence of (a) primary crystallization temperature (T_{x1}), (b) temperature difference between primary and secondary crystallization (ΔT_x), (c) mean grain size (D), (d) saturation induction (B_s), (e) activation energy (Q_{JMA}), and (f) coercivity (H_c) and permeability (μ) for alloys $\text{Fe}_{54.6}\text{Co}_{29.4}\text{Si}_{2.8}(\text{B}_{0.8-Y}\text{P}_Y)_{14}\text{Nb}_1\text{Cu}_1$ where $Y=0, 0.2,$ and 0.3 .

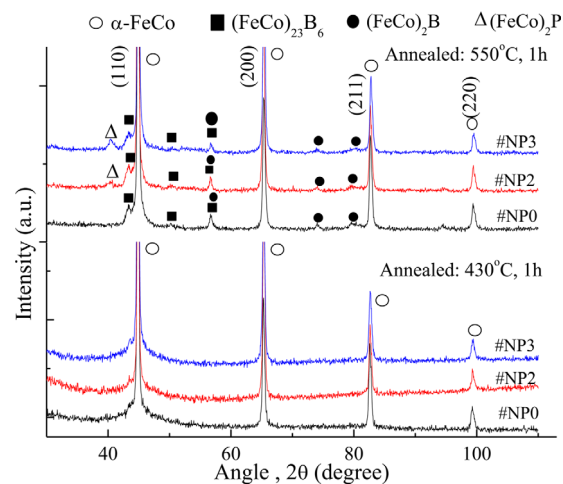


FIG. 2. (Color online) X-ray diffraction patterns of annealed melt-spun #NP0, #NP2, and #NP3 alloys.

annealing (Fig. 3). The crystalline volume fraction in nanocrystalline two-phase system of alloy #NP0 is larger than that of alloys #NP2 and #NP3, giving evidence for the enhanced amorphization with the P addition.

The increase in amorphization with P additions has been also reported in earlier research³ and can be explained by the model of Senkov *et al.*¹¹ This model reports the effect of atomic size differences of alloying elements on the structural instability in a crystalline solid solution. The structural instability occurs when the internal stress of a crystal reaches a critical level, and the internal stress is dependent on the atomic mismatch of constituents. A tensile strain is developed in the octahedral sites for $R_Y > 0.6R_X$ (where R_Y , the radius of alloying elements and R_X , the radius of matrix atoms) and a compressive strain is produced in the substitutional sites for $R_Y < 0.85R_X$. Interstitial atoms that produce tensile strains attract the substitutional atoms that are smaller than the matrix atoms. It may stabilize the amorphous state with the generation of dense and short range order atomic configuration. According to the Senkov model, due to size effects, i.e., $R_B > 0.6R_{\text{Fe}}$ and $R_P < 0.85R_{\text{Fe}}$ (where R_P is the radius of the

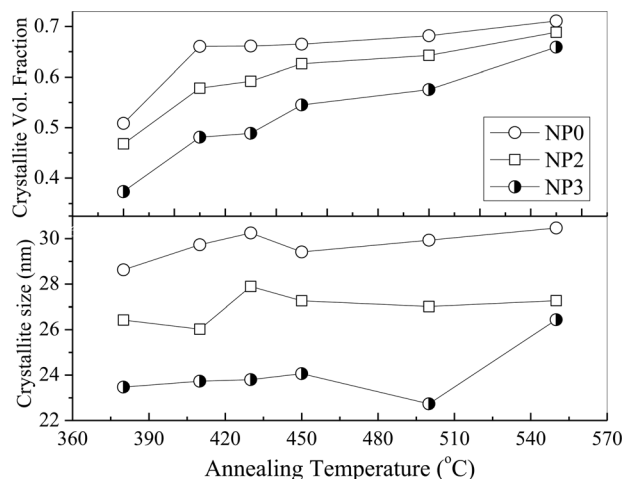


FIG. 3. Annealing temperature dependencies of crystalline volume fraction and crystalline size for melt-spun #NP0, #NP2, and #NP3 alloys.

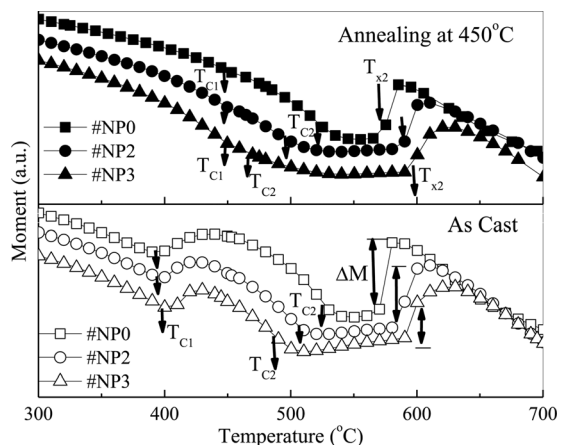


FIG. 4. Magnetic moments of as-cast and annealed (at 450 °C) alloys of #NP0, #NP2, and #NP3 as a function of temperature.

P atom, R_B is the radius of the B atom, and R_{Fe} is the radius of the Fe atom), P creates a large compressive lattice strain at the substitutional site while B causes a large tensile lattice strain in the octahedral site, and the amorphization is enhanced in P added alloys. Similar arguments have been used to describe hardening mechanisms in nanocomposites.¹²

Grain refinement can be explained in terms of the mixing enthalpy (ΔH) of the constituent elements.⁸ The negative ΔH between Cu and P (-9 kJ/mol) causes the strong attraction between the atoms, whereas positive ΔH between Fe/Co and Cu results in repulsive forces between the elements. It leads to the separation of a small region with enriched Cu and P from the amorphous matrix, and acts as the heterogeneous nucleation sites for α -FeCo, increasing grain refinement.

The magnetic moment of as-cast and annealed (450 °C) alloys changes as a function of temperature and has minimum values at two temperatures, labeled T_{c1} , T_{c2} prior to secondary crystallization (Fig. 4). The magnetization of as-quenched amorphous phase is a monotonically decreasing function of temperature, disappearing in a second order phase transition at its Curie temperatures. The magnetic moment changes at temperature T_{c1} , corresponds to the formation of α -FeCo nanocrystals with larger magnetizations through primary crystallization. The nanocrystals increase the magnetic moments of annealed alloys, resulting in the increase of the T_{c1} of post annealed (at 450 °C) alloys than that of as-cast alloys. With P addition, the stabilization of amorphous phase delays primary crystallization, resulting in a little increase of T_{c1} for #NP0, #NP2, and #NP3 as-cast alloys as a function of P. However, there is no change in T_{c1} for annealed alloys due to the formation of α -FeCo nanocrystals. The composition change during nanocrystallization acts to increase the relative concentration of glass formers in the amorphous matrix and consequently decreases the net dipole moment in this phase. The amorphous phase magnetization continues to decrease with temperature, disappearing at T_{c2} which is the Curie temperature of the residual amorphous phase. The continuous decrease and a sudden increase in magnetic moments (ΔM) during post primary

crystallization are attributed to simultaneous dissolution and re-nucleation of α -FeCo nanocrystals, respectively. The dissolution is for the recrystallization of non-magnetic $(FeCo)_{23}B_6$ phase, and the re-nucleation causes from the residual amorphous phase.

It is interesting to note some observations associated with post primary crystallization with P addition: (1) T_{c2} decreases, (2) the difference between T_{c2} and T_{x2} increases, and (3) the sudden jump in magnetic moment (ΔM) decreases. The possible explanations include lowering of crystallite volume fraction and increasing of thermal stability as a function of P content.

IV. CONCLUSIONS

The P content dependencies of the nanocrystallization behaviors and high temperature magnetic properties of the $Fe_{54.6}Co_{29.4}Si_{2.8}(B_{0.8-Y}P_Y)_{14}Nb_1Cu_1$ ($Y = 0, 0.2, \text{ and } 0.3$) alloys have been investigated. It was observed that the P addition increases not only thermal stability but also amorphization, grain refinement, and activation energy for secondary crystallization. Consequently, the soft magnetic properties are also enhanced for P added alloys. The saturation induction reaches the highest value of 1.68 T for as-cast P free alloy and continuously decreases with the addition of P. The stabilization of amorphous phase delays primary crystallization, resulting in a small increase of T_{c1} in the as-quenched alloys. However, the Curie temperature (T_{c2}) of residual amorphous phase decreases as a function of P content.

ACKNOWLEDGMENTS

R. K. Roy acknowledges the Department of Science and Technology (DST), Government of India and Director, CSIR-NML, for conducting this research under the BOYSCAST fellowship.

- ¹J. Long, M. E. McHenry, D. Urciuoli, V. Keylin, J. Huth, and T. Salem, *J. Appl. Phys.* **103**, 07E705 (2008).
- ²A. Urata, H. Matsumoto, S. Yoshida, and A. Makino, *J. Alloys Compd.* **509**, S431 (2011).
- ³A. Makino, H. Men, K. Yubuta, and T. Kubota, *J Appl. Phys.* **105**, 013922 (2009).
- ⁴T. Kubota, A. Makino, and A. Inoue, *J. Alloys Compd.* **509**, S416 (2011).
- ⁵R. K. Roy, A. K. Panda, M. Ghosh, A. Mitra, and R. N. Ghosh, *J. Magn. Mater.* **321**, 2865 (2009).
- ⁶M. A. Willard, D. E. Laughlin, M. E. McHenry, D. Thoma, K. Sickafus, J. O. Cross, and V. G. Harris, *J. Appl. Phys.* **84**, 6773 (1998).
- ⁷K. J. Miller, A. Leary, S. J. Kernion, A. Wise, D. E. Laughlin, M. E. McHenry, V. Keylin, and Joe Huth, *J Appl. Phys.* **107**, 09A316 (2010).
- ⁸S. J. Kernion, K. J. Miller, S. Shen, V. Keylin, J. Huth, and M. E. McHenry, *IEEE Trans. Magn.* **47**, 3452 (2011).
- ⁹A. Makino, T. Bitoh, A. Inoue, and T. Masumoto, *Scr. Mater.* **48**, 869 (2003).
- ¹⁰A. Hsiao, Z. Turgut, M. A. Willard, E. Selinger, M. Lee, D. E. Laughlin, M. E. McHenry, and R. Hasegawa, *Mater. Res. Soc. Symp. Proc.* **577**, 551 (1999).
- ¹¹O. N. Senkov and D. B. Miracle, *Mater. Res. Bull.* **36**, 2183 (2001).
- ¹²C.-Y. Um, F. Johnson, M. Simone, J. Barrow, and M. E. McHenry, *J. Appl. Phys.* **97**, 10F504 (2005).